Supporting Information

Trapping of Copper Hydride Intermediates with CO_2

Alexander Grasruck,[1] Giorgio Parla,[1] Lisha Lou,[1] Jens Langer,[1] Christian Neiß,[2] Alberto Herrera,[1] Sybille Frieß,[1] Andreas Görling,[2] Günter Schmid,[3] Romano Dorta[1]

[1)] *Department Chemie und Pharmazie, Anorganische und Allgemeine Chemie, Friedrich-Alexander-Universität Erlangen-Nürnberg, Egerlandstraße 1, 91058 Erlangen, Germany.*

[2)] *Department Chemie und Pharmazie, Theoretische Chemie, Friedrich-Alexander-Universität Erlangen-Nürnberg, Egerlandstraße 3, 91058 Erlangen, Germany*

[3)] *Siemens Energy Global GmbH & Co. KG, New Energy Business – Technology & Products Freyeslebenstraße 1, 91058 Erlangen, Germany*

Experimental details

General considerations. All reactions were carried out under anaerobic and anhydrous conditions, using standard Schlenk and glovebox techniques, unless otherwise stated. THF and benzene were distilled from purple Na/Ph_2CO solutions, *n*-pentane from Na/Ph_2CO/tetraglyme. C_6D_6 and THF-D_8 were distilled from NaK_2 alloy. KEt_3BH (1.0 M in THF, Sigma-Aldrich) was used as received. **7** and **8** were prepared according to published procedures.[1] NMR spectra were recorded on JOEL EX 400 (400.5 MHz), JOEL EX 270 (270 MHz), and Bruker Avance DPX300 NB (300 MHz) spectrometers, and the solvent residual signals were used as internal reference for the ^{1}H NMR spectra.[2] The raw NMR data were processed with Mestrec. Elemental analyses (EA) were performed on a Euro EA 3000 analyzer, and air-sensitive samples were handled in a glovebox. UV-Vis spectra were recorded on a UV/VIS SPECORD S600 (Analytik Jena AG) spectrophotometer.

***In situ* formation of [CuH(KClBEt$_3$)(5-(diisopropylphosphanyl)-5*H*-dibenzo[*b,f*]azepine)$_2$] (10). a) for UV-Vis measurement:** The preparation of the complex and the measurements were conducted in an inert gas glovebox and the temperature was kept below –30°C at all times. All solvents and solutions were precooled to -30°C in a cold trap with liquid nitrogen as cooling agent. The UV-Vis cuvette (*d* = 1 cm) containing the solution of the complex was kept at –30°C during the measurement. 2 mL injection syringes (B. Braun), 100µL Eppendorf Research® plus pipette and Eppendorf pipette tips were used to transfer the solutions and solvents. 100µL of a colourless 0.059 M solution of KEt_3BH in THF was added to 900µL of a colorless solution of **8** in THF (0.0064 M) to afford a bright yellow 0.0058 M solution of

complex **10**. This solution was twice diluted tenfold with fresh THF to form a 5.8×10^{-5} M solution, of which 700µL were combined with 2.5mL THF and transferred to a UV-VIS cuvette for the final 1.3×10^{-5} M solution. **b) for NMR spectroscopy:** All solutions were handled and kept below –30 ºC at all times. **8** (20 mg, 0.028 mmol) was dissolved in THF-d_8 (0.6 mL) and cooled to –30 °C. A solution of KEt_3BH (0.25 ml, 0.250 mmol, 1.0 M in THF) was added *via* syringe. The solution immediately turned yellow and then was subjected to NMR spectroscopy.

[Cu(OCHOBEt$_3$)(5-(diphenylphosphanyl)-5*H*-dibenzo[*b,f*]azepine)$_2$] (11): 7 (101 mg, 0.120 mmol) was dissolved in THF and cooled to -65 °C in an EtOH/N_2(l) cooling-bath. A solution of KEt_3BH (0.110 ml, 1.10 mmol, 1.0 M in THF) was added via gas tight syringe. The color changed immediately to yellow, and temperature was slowly raised to -35 °C. CO_2 gas was channeled through the reaction mixture for 10 min, while the color lightened, and the formation of a precipitate was observed. The solvent was removed at -25 °C and brought inside a glove box. The product was extracted with cold toluene (-30 °C) and centrifuged to separate the solution from the KCl precipitate. The colorless solution was cooled to -35 °C and the solvent was removed to afford a glue, which was washed and slurried with cold n-pentane (3 ml) to afford an off-white powder (168 mg, 94 %). ^{1}H NMR (400 MHz, C_6D_6) δ (ppm) = 8.53 (s, 1H), 7.35 (d, *J* = 7.0 Hz, 8H), 7.16 (d, *J* = 7.6 Hz, 4H), 7.08-6.89 (m, 13H), 6.87-6.56 (m, 13H), 6.28 (s, 4H), 1.45 (t, *J* = 7.7 Hz, 9H), 1.17 (q, *J* = 7.7 Hz, 6H). ^{31}P{^{1}H} NMR (162 MHz, C_6D_6) δ (ppm) 61.21 (s). ^{11}B NMR (128 MHz, C_6D_6) δ (ppm) = - 4.91 (s, br). ^{13}C NMR (101 MHz, C_6D_6) δ (ppm) = 169.85 (s), 146.77 (s), 137.26 (s), 133.48 (s), 131.54 (s), 129.52 (s), 129.30 (s), 129.05 (s), 127.64 (s), 126.15 (s), 17.40 (s), 9.72 (s). IR (KBr, cm^{-1}): ν = 3060 (m), 3026 (w), 2940 (m), 2900 (w), 2860 (m), 2806 (w), 1615 (vs), 1484 (m), 1488 (m), 1433 (m), 1355 (w), 1280 (w), 1240 (w), 1204 (m), 1103 (m), 1040 (w), 970 (m), 798 (m), 750 (m), 700 (m), 550 (m), 494 (m). EA: found C 73.32%, H 5.81%, N 2.79%; calculated for $C_{59}H_{56}BN_2P_2CuO_2$: C 73.71%, H 5.81%, N 2.91%.

[Cu(OCHOBEt$_3$)(5-(diisopropylphosphanyl)-5*H*-dibenzo[*b,f*]azepine)$_2$] (12): 8 (181 mg, 0.252 mmol) was dissolved in THF and cooled to -65 °C in an EtOH/N_2(l) bath. A solution of KEt_3BH (0.25 ml, 0.250 mmol, 1.0 M in THF) was added via gas tight syringe. The color changed immediately to yellow, and temperature was slowly raised to -35 °C. CO_2 gas was channeled through the reaction mixture for 10 min, while the color lightened, and the formation of a precipitate was observed. The solvent was removed at -30 °C and the reaction vessel brought inside a glove box. The product was extracted with cold toluene (-30 °C, filtration over GF/B) and the brownish cooled solution (-35 °C) was evaporated to a brown glue, which was washed and slurried with cold n-pentane (3 ml) to yield a white powder (164 mg, 78 %). ^{1}H NMR (400 MHz, C_6D_6) δ (ppm) = 8.97 (s, 1H), 7.33 (d, *J* = 8.1 Hz, 4H), 7.17 (t, *J* = 7.6 Hz, 4H), 6.87-6.60 (m, 8H), 6.42 (s, 4H), 1.57-1.39 (m, 13H), 1.19 (q, *J* = 7.7 Hz, 6H),

0.94 (br. s, 12H), 0.81 (br. s, 12H). $^{31}P\{^1H\}$ NMR (162 MHz, C_6D_6) δ (ppm) = 86.46 (s). ^{13}C NMR (101 MHz, C_6D_6) δ (ppm) = 169.84 (s), 147.27 (s), 135.79 (s), 131.75 (s), 130.48 (s), 129.39 (s), 125.78 (s), 28.07 (s), 18.68 (s), 17.71 (s), 16.09 (s), 10.75 (s). EA: found C 67.41%, H 6.92%, N 3.75%; calculated for $C_{47}H_{64}BN_2P_2CuO_2$: C 67.70%, H 6.79%, N 3.85%.

[Cu(HCO$_2$)(5-(diisopropylphosphanyl)-5*H*-dibenzo[*b,f*]azepine)$_2$] (13): Complex **12** was prepared as described above from **8** (228 mg, 0.318 mmol) and then recrystallized by dissolving it in C_6H_6 (2 ml) and layering with n-pentane (3 ml). This afforded colorless X-ray quality crystals (111 mg, 48%) over the course of 10 d. ^1H NMR (400 MHz, C_6D_6) δ (ppm) = 9.39 (s, 1H), 7.49 (d, *J* = 8.0 Hz, 4H), 7.21-7.11 (m, 4H), 6.88-6.64 (m, 8H), 6.45 (s, 4H), 1.72- 1.48 (m, 4H), 1.23-1.06 (m, 12H), 0.92 (dd, *J* = 15.8, 7.0 Hz, 12H). $^{31}P\{^1H\}$ NMR (162 MHz, C_6D_6) δ (ppm) = 85.62 (s). ^{13}C NMR (101 MHz, C_6D_6) δ (ppm) = 168.04 (s), 147.63 (s), 135.94 (s), 131.80 (s), 130.23 (s), 129.26 (s), 128.13 (s), 125.57 (s), 28.35 (d, *J* = 6.1 Hz), 18.54 (d, *J* = 9.4 Hz), 18.07 (s). EA found C 67.41%, H 6.92%, N 3.75%; calculated for $C_{41}H_{49}N_2P_2CuO_2$ containing 0.1 equiv $C_{40}H_{48}N_2P_2CuCl$: C 67.63%, H 6.79%, N 3.86%.

X-ray diffraction analysis: A suitable crystal of compound **11** or **13** was embedded in inert perfluoropolyalkylether (viscosity 1800 cSt; ABCR GmbH) and mounted using a Hampton Research CryoLoop. The selected crystal was then flash cooled to 100°K in a nitrogen gas stream and kept at this temperature during the experiment. The crystal structures were measured on an Agilent SuperNova diffractometer with Atlas S2 detector using a CuKα microfocus source. The measured data were processed with the CrysAlisPro software package.[3] Using Olex2,[4] the structures were solved with the ShelXT[5] structure solution program using Intrinsic Phasing and refined with the ShelXL[6] refinement package using Least Squares Minimization. All non-hydrogen atoms were refined anisotropically. All hydrogen atoms were placed in ideal positions and refined as riding atoms with relative isotropic displacement parameters. In the case of compound **11**, three symmetry-independent molecules per asymmetric unit were observed and a channel filled with a non-stoichiometric amount of benzene solvent molecules was detected in the middle of the unit cell. The structure suffers from substantial disorder of all BEt_3 moieties and of the co-crystallized benzene molecules. In one of the three molecules of **11**, additional disorder of the central $(PhP)_2Cu$ formate subunit was found. A suitable disorder model was built with the help of similarity restraints (SIMU, SADI) and rigid bond restraints (RIGU).[7] Furthermore, some of the disordered benzene molecules were treated as idealized hexagons (AFIX 66). The data of compound **13** showed substitutional disorder between the formate moiety and residual chloride from the starting material **8**. An ISOR restraint was placed on the Cl atom to facilitate refinement and a ratio of 89 to 11 between HCO_2^- and Cl^- was determined for the measured crystal. Crystallographic and refinement data for **11** and **13** are summarized in Table S1.

The crystal structure data of the compounds has been deposited with the Cambridge Crystallographic Data Centre. CCDC 2265253 (**11**) and 2265254 (**13**) contain the supplementary crystallographic data, which can be obtained free of charge from The Cambridge Crystallographic Data Centre via www.ccdc.cam.ac.uk/data_request/cif.

Table S1. Crystal data and structure refinement for compounds **11** and **13**

Compound	**11**·1.429 C_6H_6	**13**[a]
Identification code	rodo181018c	rodo190905b
Empirical formula	$C_{67.58}H_{64.58}BCuN_2O_2P_2$	$C_{40.89}H_{48.89}Cl_{0.11}CuN_2O_{1.78}P_2$
Formula weight	1072.97	726.29
Temperature/K	100.0(1)	100.0(2)
Crystal system	triclinic	orthorhombic
Space group	P-1	$P2_12_12_1$
a/Å	14.3056(2)	10.29438(6)
b/Å	22.4286(3)	15.43040(8)
c/Å	28.0190(3)	23.74742(11)
α/°	76.2750(10)	90
β/°	78.6300(10)	90
γ/°	78.9470(10)	90
Volume/Å^3	8462.19(19)	3772.19(3)
Z	6	4
ρ_{calc}g/cm^3	1.263	1.279
μ/mm^{-1}	1.442	1.963
F(000)	3384.0	1533.0
Crystal size/mm^3	0.385 × 0.338 × 0.121	0.224 × 0.19 × 0.1
Radiation	CuKα (λ = 1.54184)	Cu Kα (λ = 1.54184)
2Θ range for data collection/°	6.376 to 147.552	6.832 to 145.35
Index ranges	$-17\leq h\leq 17$, $-27\leq k\leq 27$, $-34\leq l\leq 34$	$-12\leq h\leq 9$, $-19\leq k\leq 18$, $-29\leq l\leq 28$
Reflections collected	126024	28583
Independent reflections	32991	7366
R_{int}/R_{sigma}	0.0289/0.0245	0.0375/0.0275
Data/restraints/parameters	32991/1592/2488	7366/6/451
Goodness-of-fit on F^2	1.038	1.028
Final R indexes [I>=2σ (I)]	R_1 = 0.0495, wR_2 = 0.1258	R_1 = 0.0317, wR_2 = 0.0827
Final R indexes [all data]	R_1 = 0.0604, wR_2 = 0.1358	R_1 = 0.0319, wR_2 = 0.0829
Largest diff. peak/hole / e Å^{-3}	0.70/-0.64	0.44/-0.41
Flack parameter	-	0.010(7)

[a]) contains 11% of [CuCl(5-(diisopropylphosphanyl)-*5H*-dibenzo[*b,f*]azepine)$_2$] (**8**) as impurity.

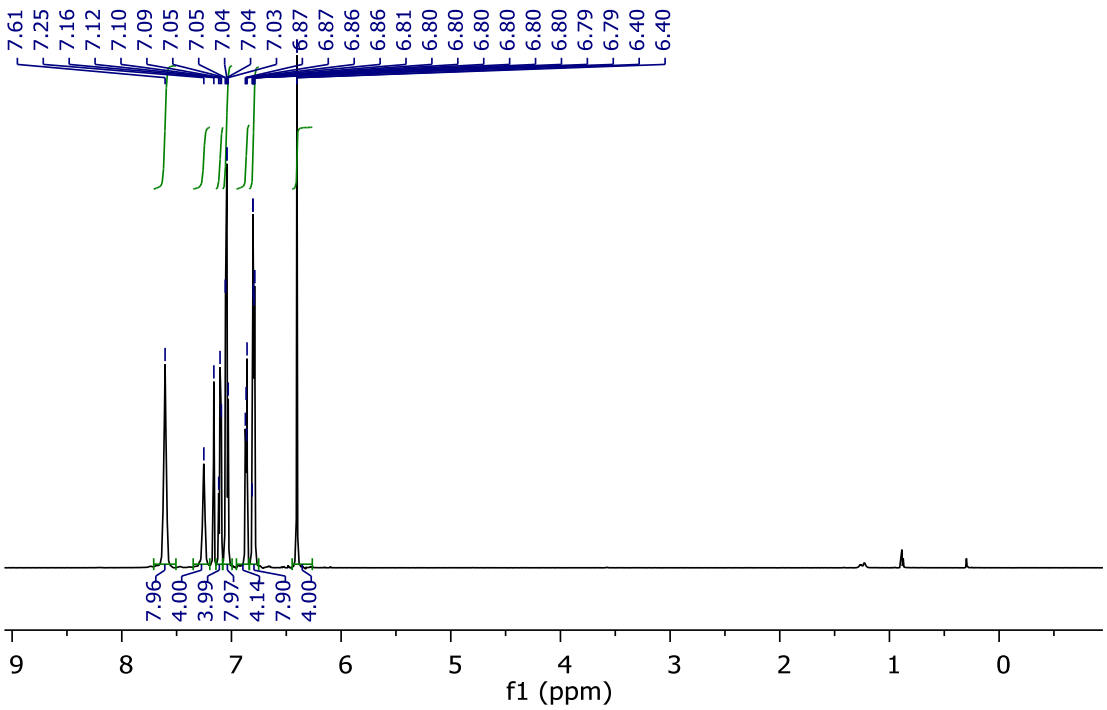

Figure S1: ^{1}H NMR of **7** in C_6D_6.

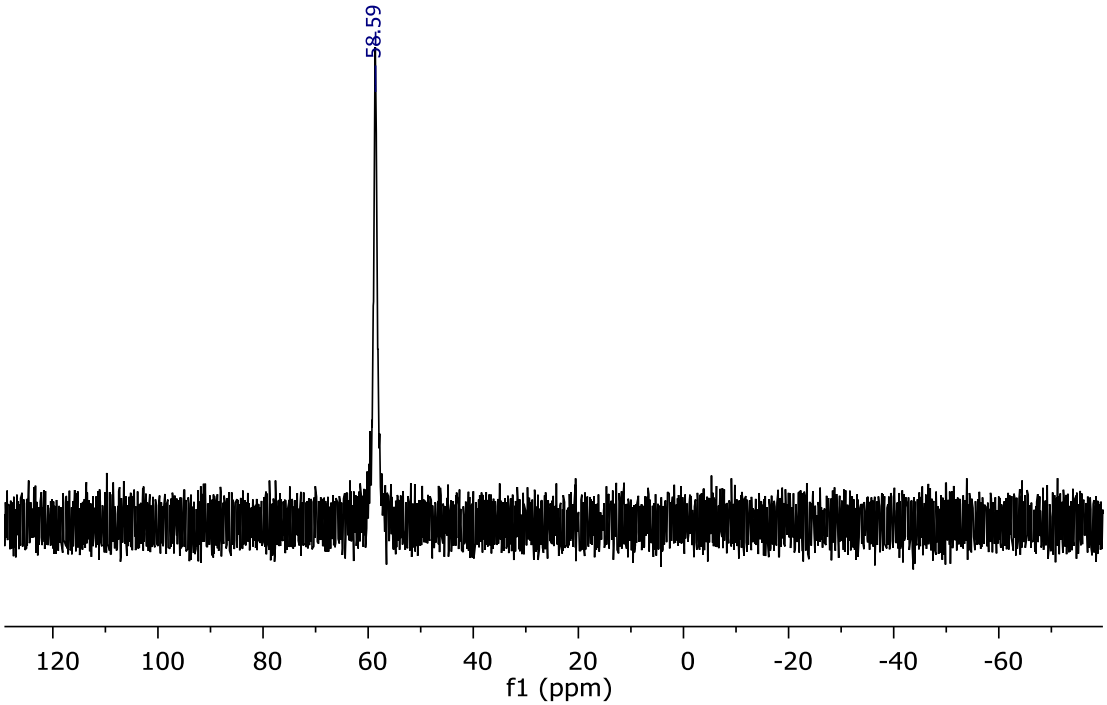

Figure S2: ^{31}P NMR of **7** in C_6D_6.

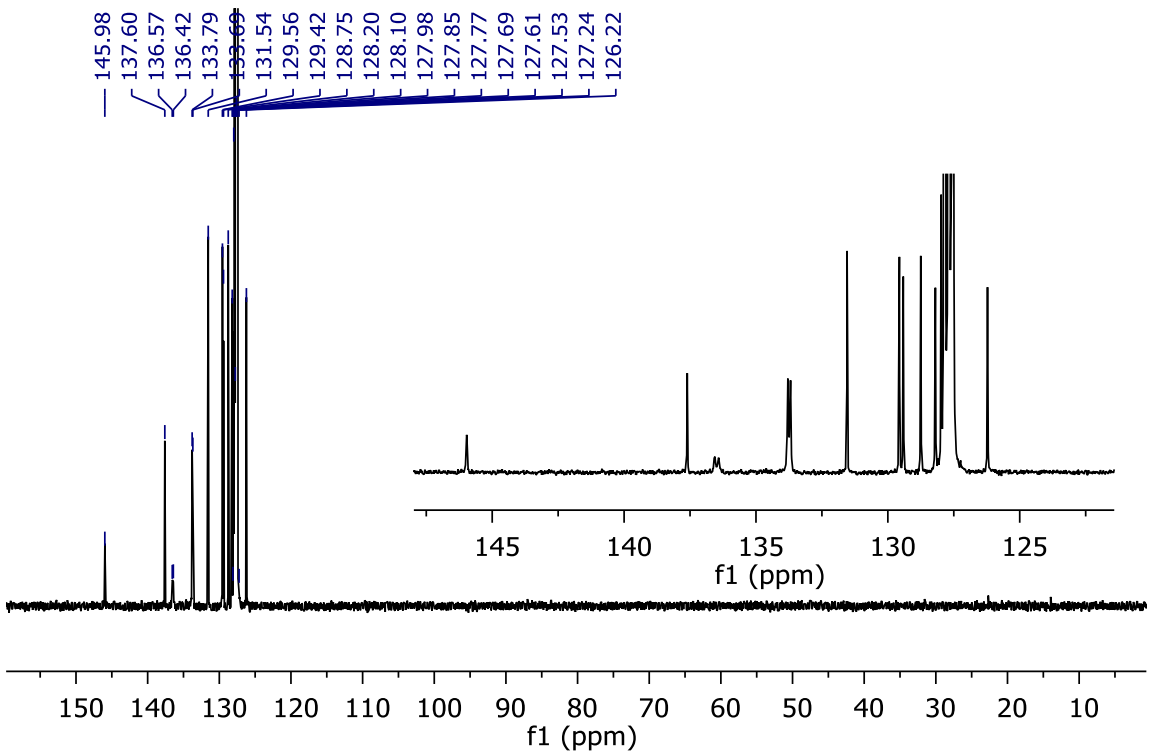

Figure S3: ^{13}C of **7** in C_6D_6.

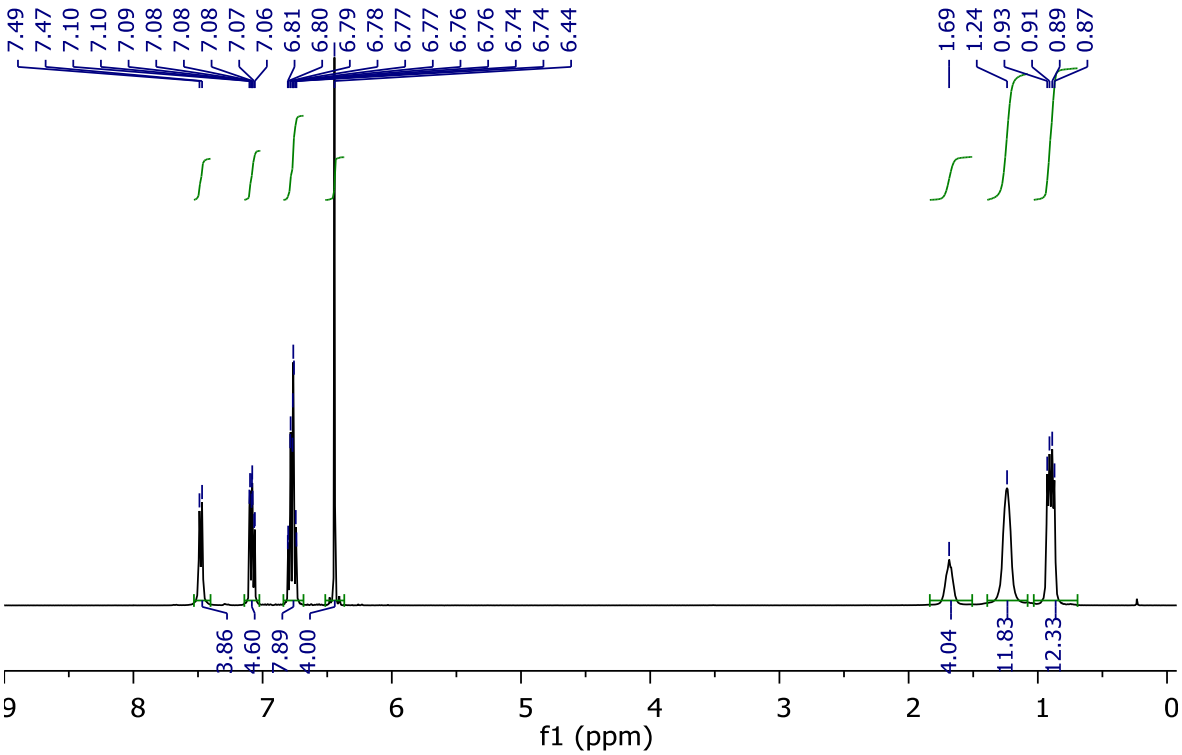

Figure S4: ^{1}H NMR of **8** in C_6D_6.

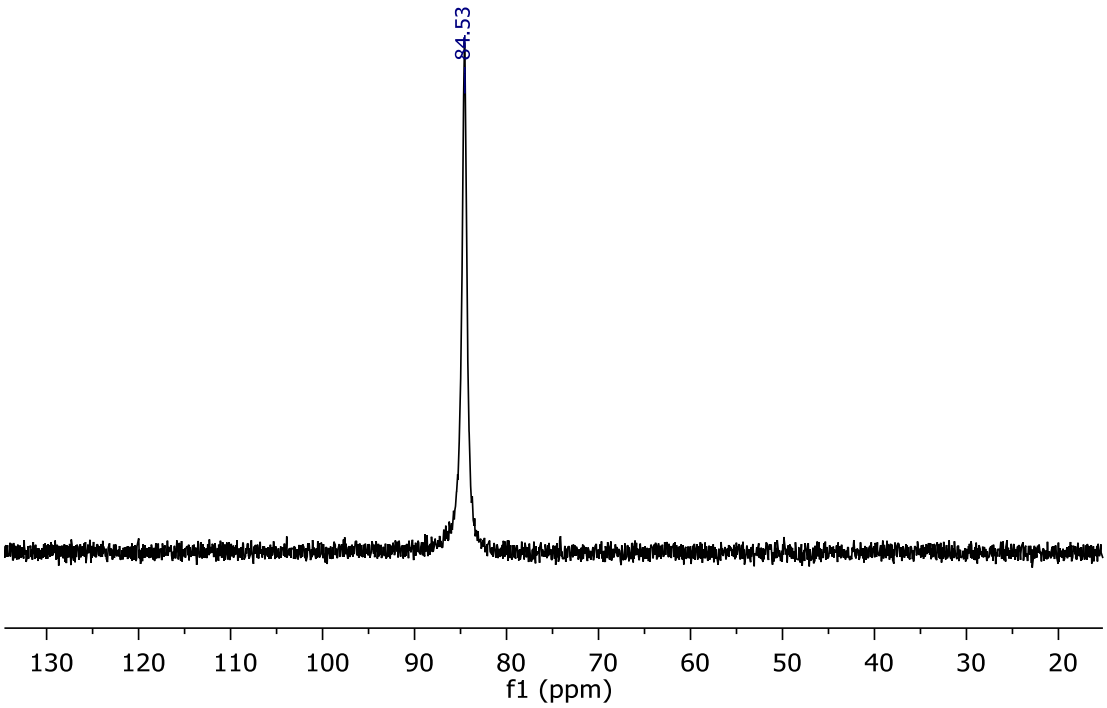

Figure S5: ^{31}P NMR of **8** in C_6D_6.

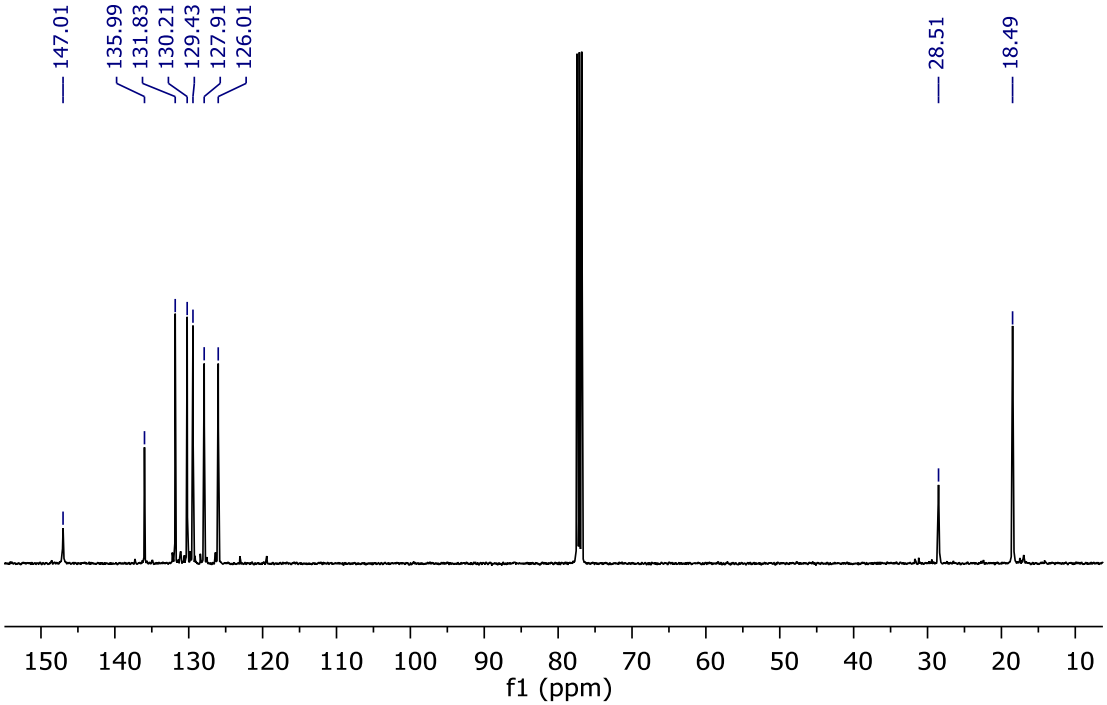

Figure S6: ^{13}C NMR of **8** in $CDCl_3$.

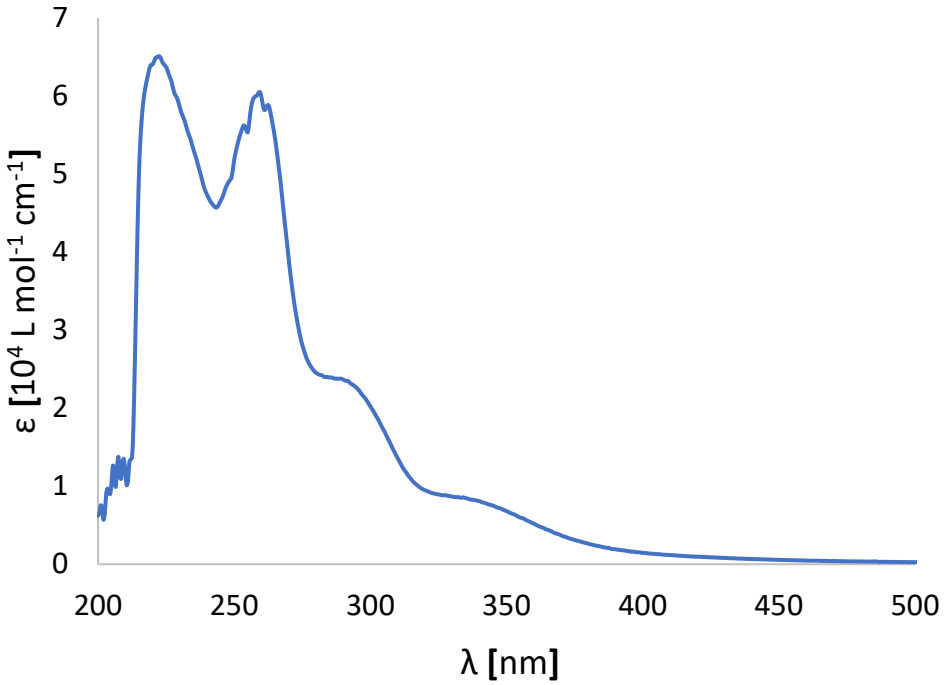

Figure S7: UV-Vis spectrum of **10** recorded in THF solution at –30°C

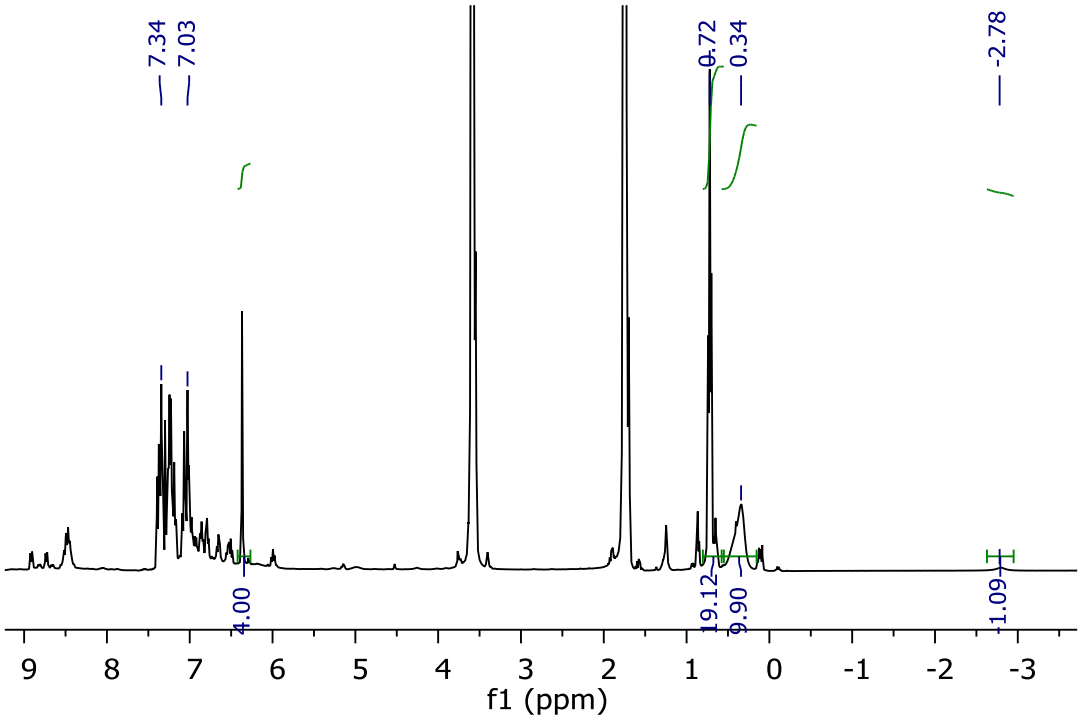

Figure S8: ^{1}H NMR of **10** in THF-d_8 at -40°C

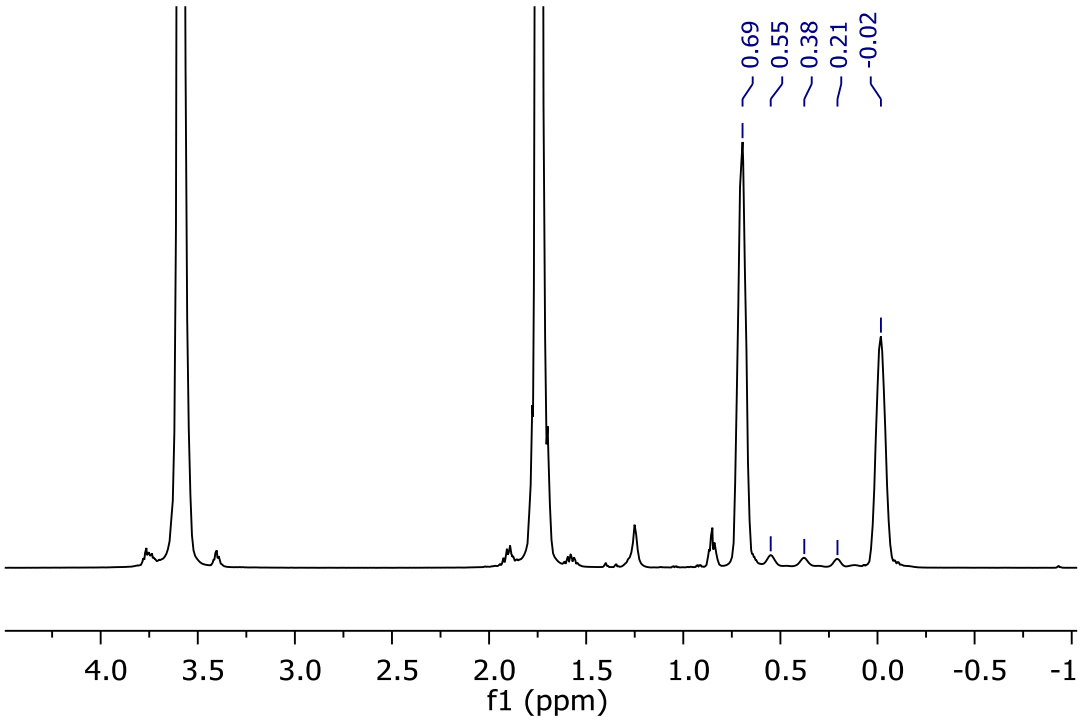

Figure S9: ^{1}H NMR of commercial 1M $KHBEt_3$ in THF-d_8 at -40°C

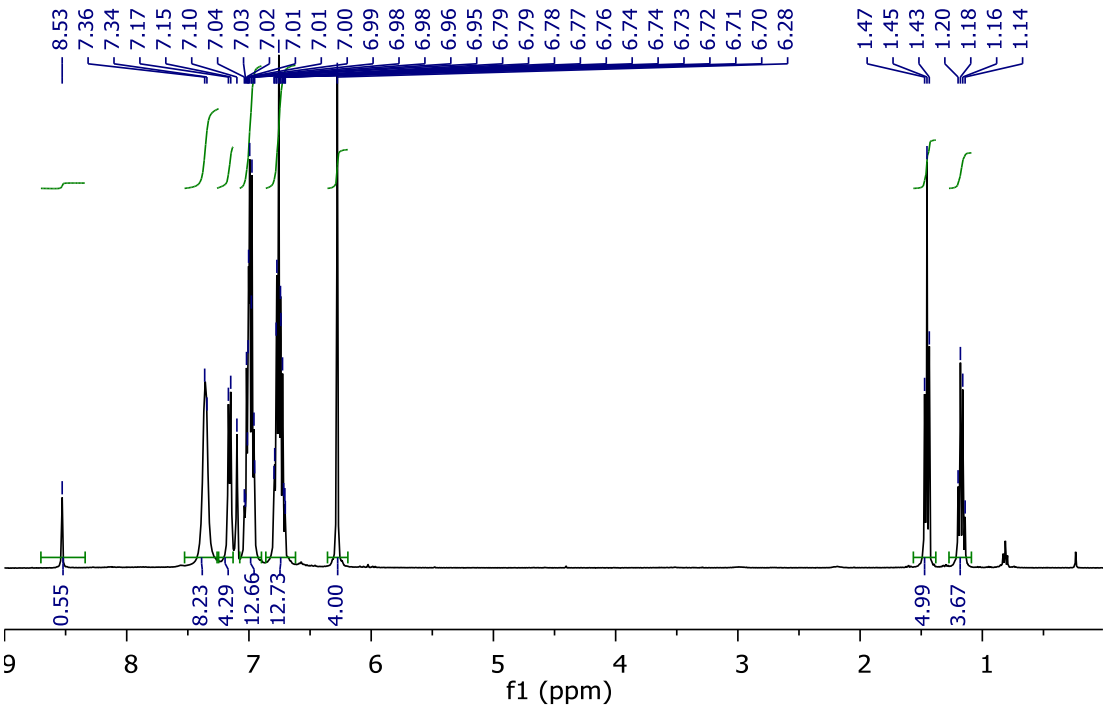

Figure S10: ^{1}H NMR of **11** in C_6D_6.

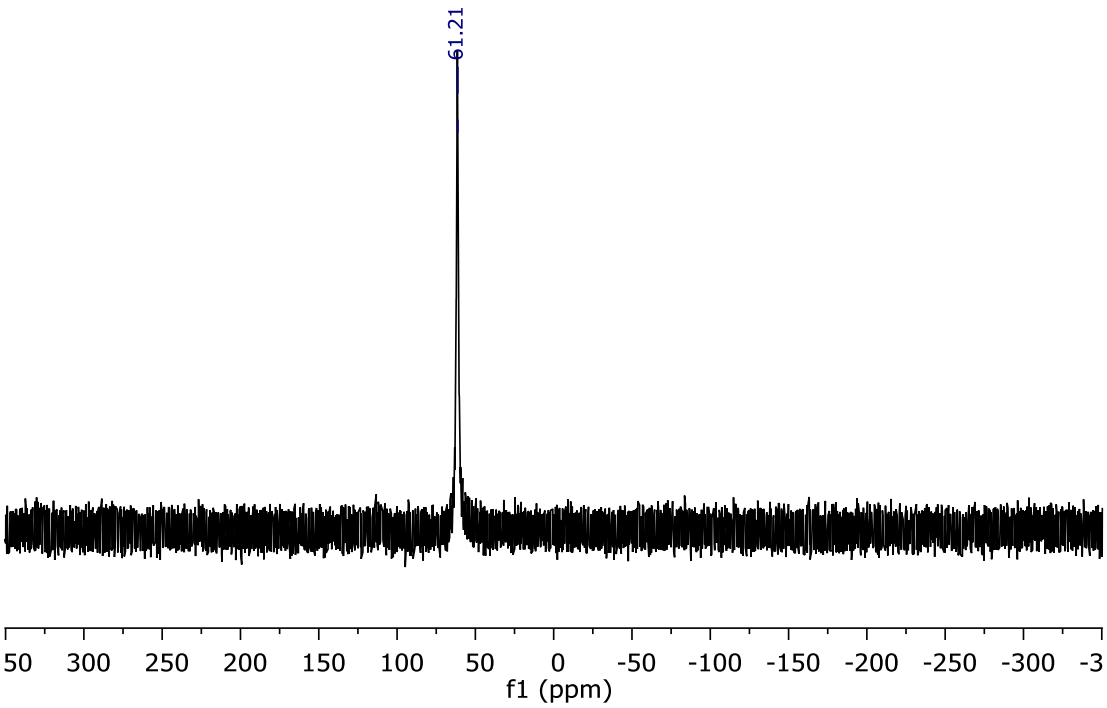

Figure S11: ^{31}P NMR of **11** in C_6D_6.

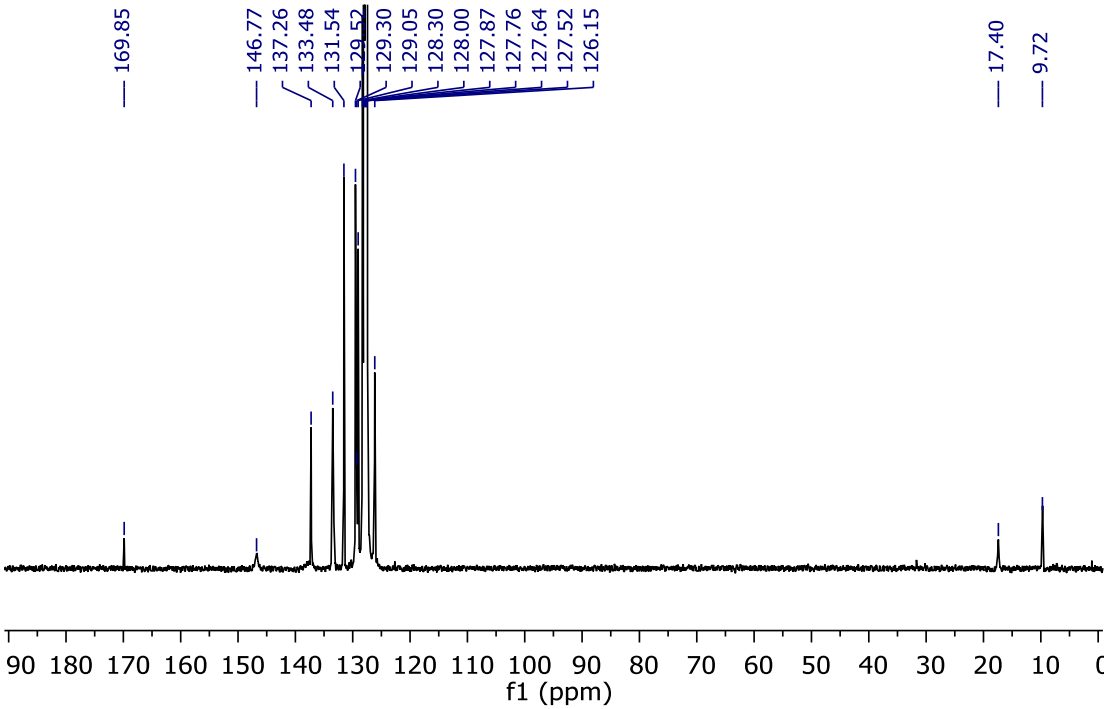

Figure S12: ^{13}C NMR of **11** in C_6D_6.

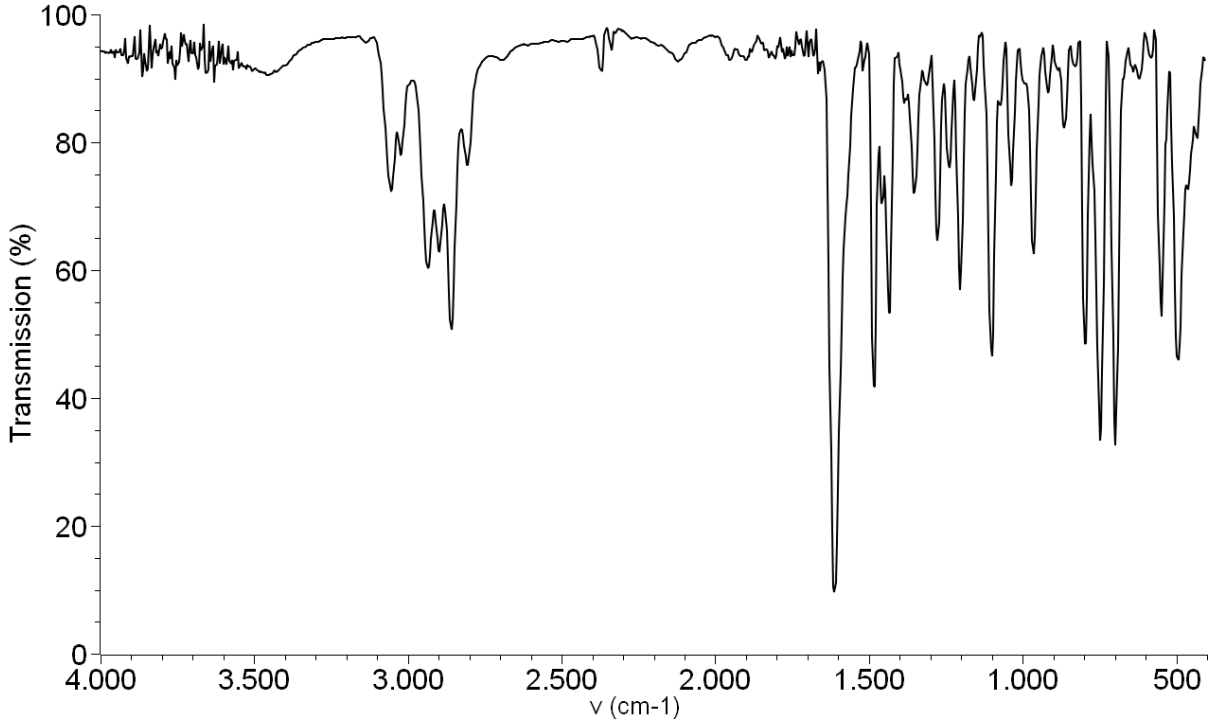

Figure S13: IR spectrum of **11**, KBr pellet

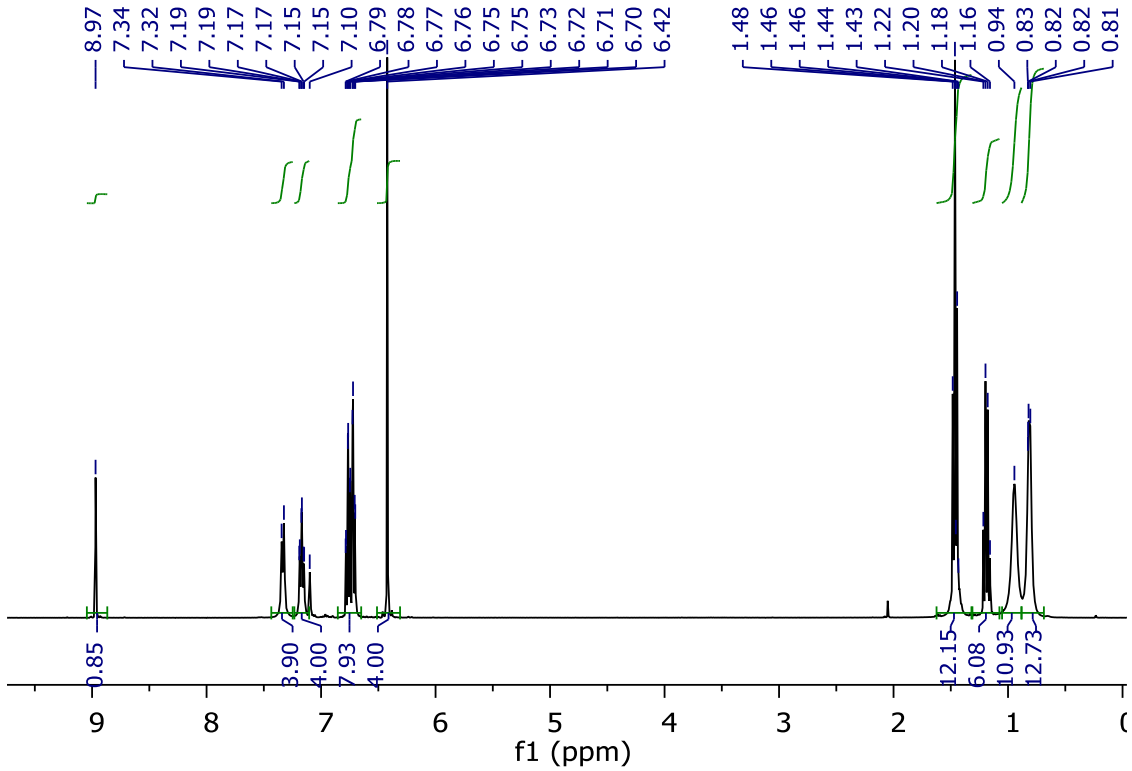

Figure S14: ^{1}H NMR of **12** in C_6D_6.

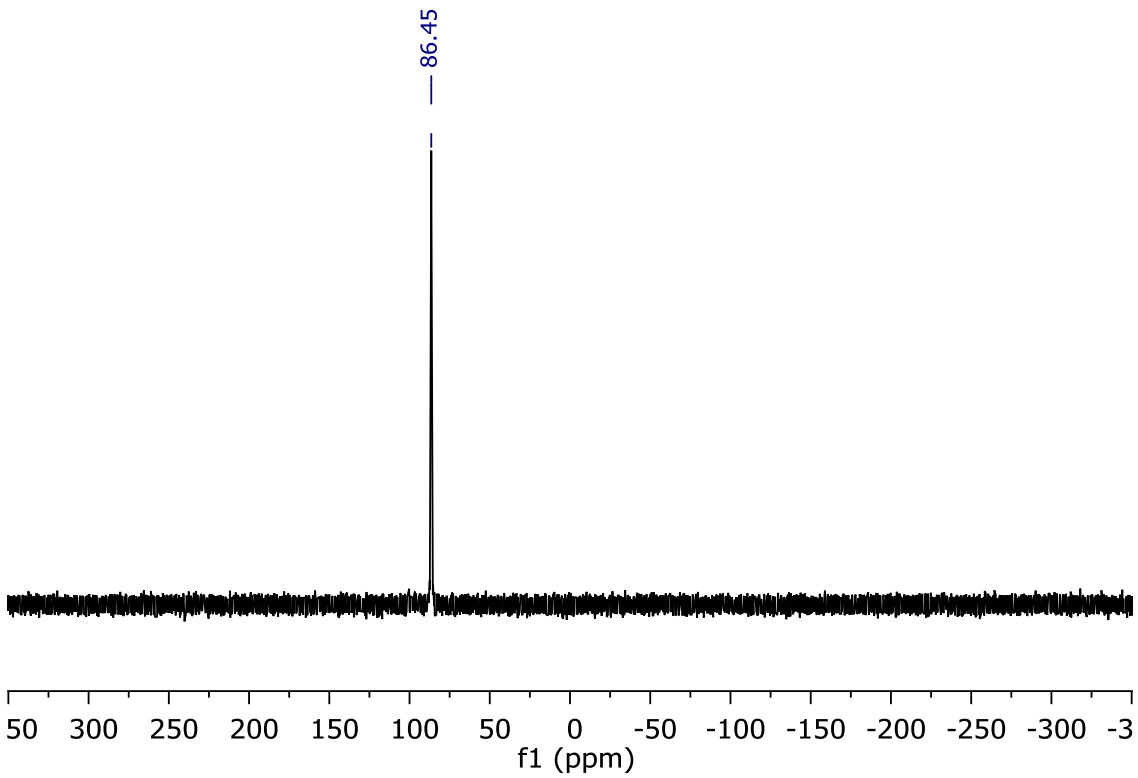

Figure S15: ^{31}P NMR of **12** in C_6D_6.

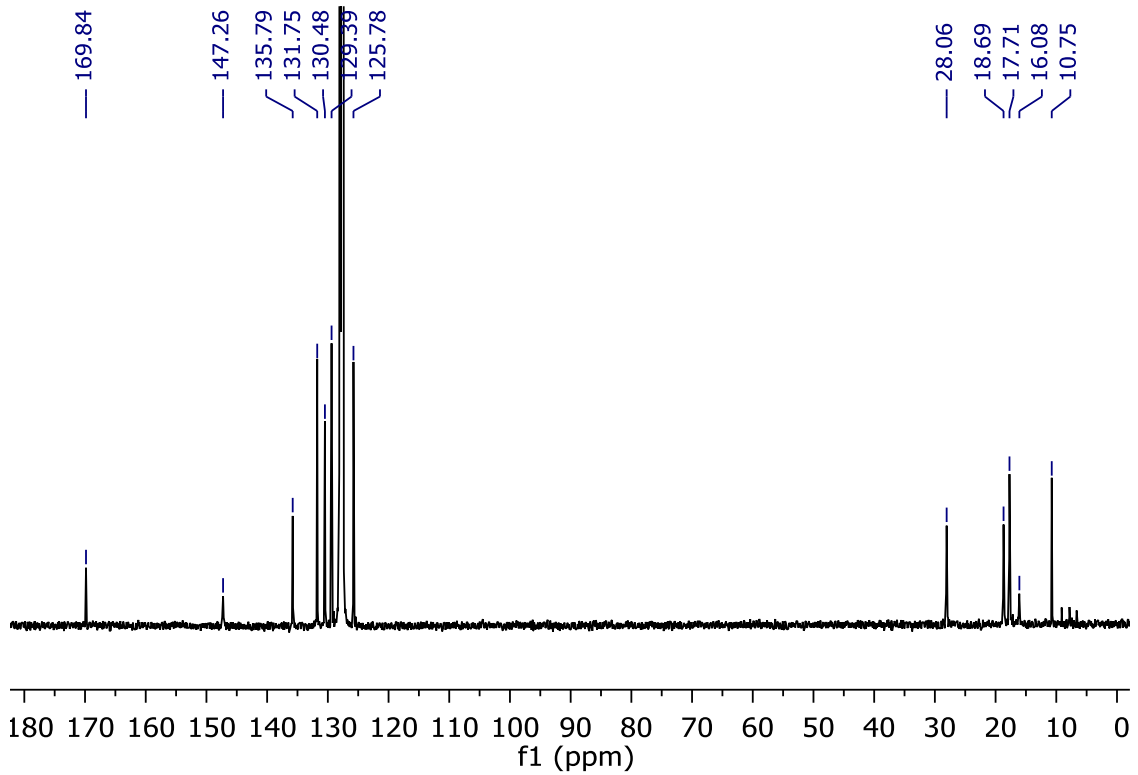

Figure S16: ^{13}C NMR of **12** in C_6D_6.

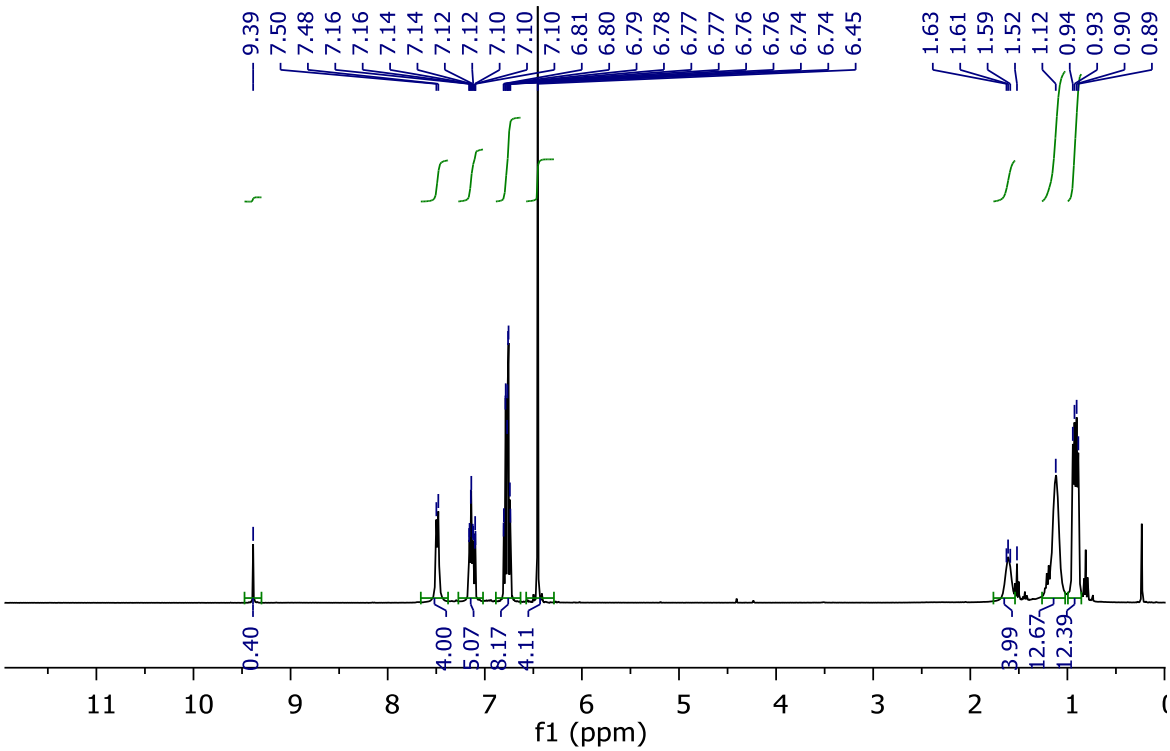

Figure S17: ^{1}H NMR of **13** in C_6D_6.

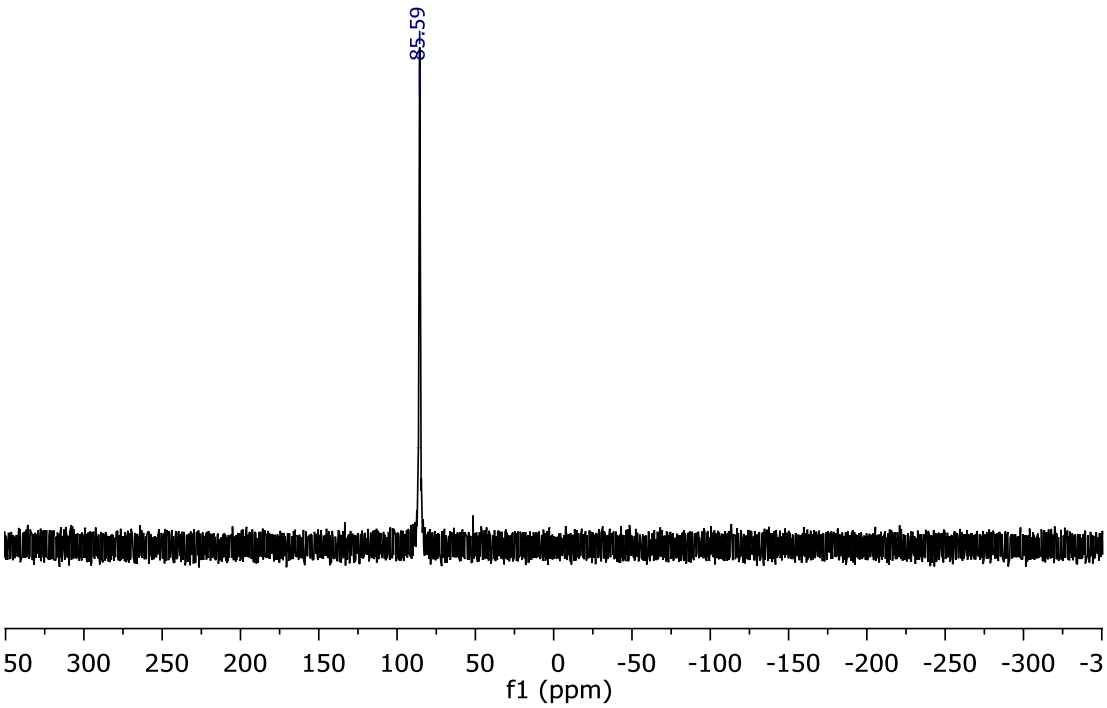

Figure S18: ^{31}P NMR of **13** in C_6D_6.

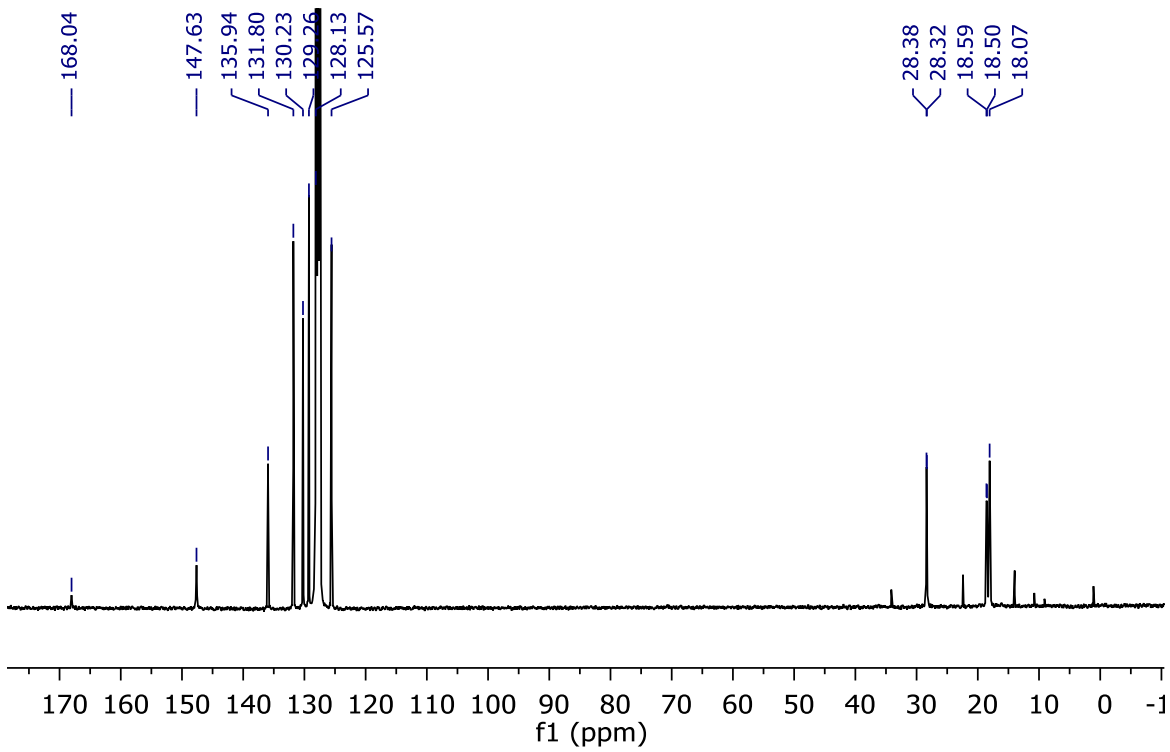

Figure S19: ^{13}C NMR of **13** in C_6D_6.

Computational Details

All quantum mechanical calculations were performed using ORCA 5.0.3.[8] Geometries were optimized on the BP86 level[9] including the van-der-Waals interaction correction according to Grimme v4 (D4 dispersion correction).[10] Throughout, basis sets from the def2-TZVP library[11] were used and the RI method was employed to calculate the Coulomb part of the electronic energy.[12] Solvent effects were considered using the conductor-like polarizable continuum model (C-PCM)[13] mimicking THF with an dielectric constant $\varepsilon = 7.25$ and an refractive index $n = 1.407$. Thermal contributions to the Gibbs energy are computed at T = 200 K (-73 °C) adopting the quasi Rigid Rotor Harmonic Oscillator approximation (qRRHO) as devised by Grimme.[14] Final electronic energies were obtained by a single-point energy evaluation at the optimized geometries (see above) employing the double-hybrid density-functional B2GP-PLYP-D3[15] (def2-TZVP basis set). Following common conventions, we denote this level of theory as B2GP-PLYP-D3/TZVP//BP84-D4/TZVP. Exact exchange contributions were treated within the COSX approximation[16] and two-electron correlation integrals again with the RI approximation.[17] We note in passing that all considered reaction energies differ by less than 4 kcal/mol from the energies

computed at the BP86-D4/TZVP level (which was used for the geometry optimizations, see above). Atomic charges were computed from a Mayer population analysis based on the BP86-D4/TZVP electron densities.[18] Electronic excitation energies were computed on the time-dependent double-hybrid density-functional approximation (TD-DHDFA) level including CIS(D)-like doubles corrections using the SCS-B2GP-PLYP21 double-hybrid functional according to Casanova-Páez and Goerigk,[19] which is by design optimized for excited states. The Tamm-Dancoff approximation (TDA) was switched off. Both the B2GP-PLYP-D3 single-point and the TD-DHDFA calculations comprised the C-PCM model as described above. Figures S20-S24 show the optimized structures of copper-hydrido species **10a**–**10d**.

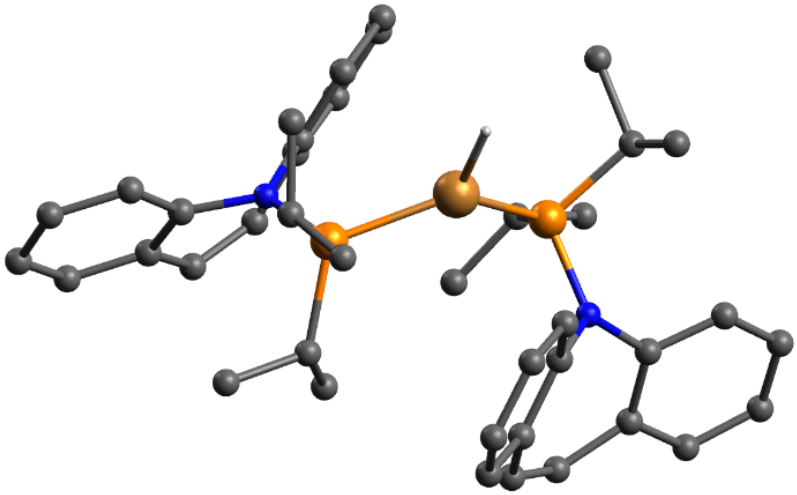

Figure S20: Optimized structure of **10a** on the BP86-D4/def2-TZVP level of theory.

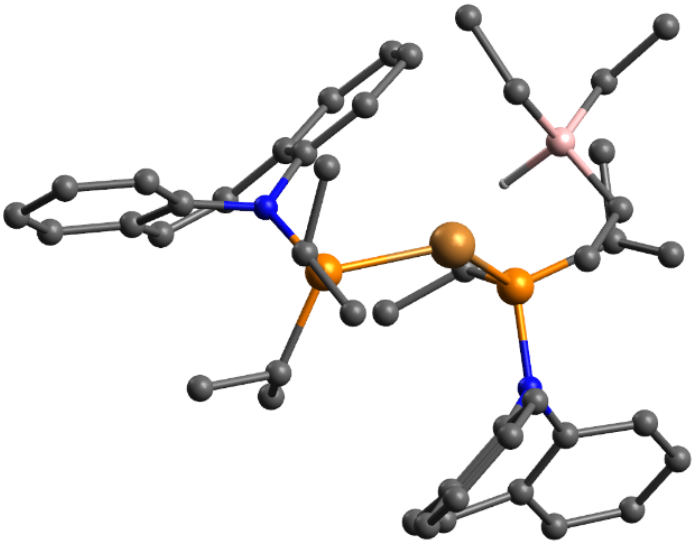

Figure S21: Optimized structure of **10b** on the BP86-D4/def2-TZVP level of theory.

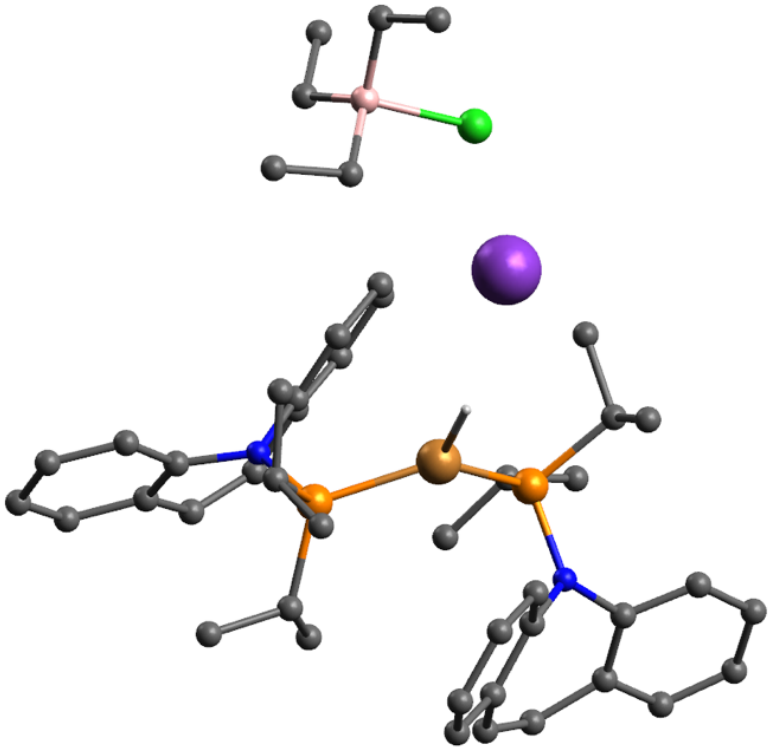

Figure S22: Optimized structure of **10c** on the BP86-D4/def2-TZVP level of theory.

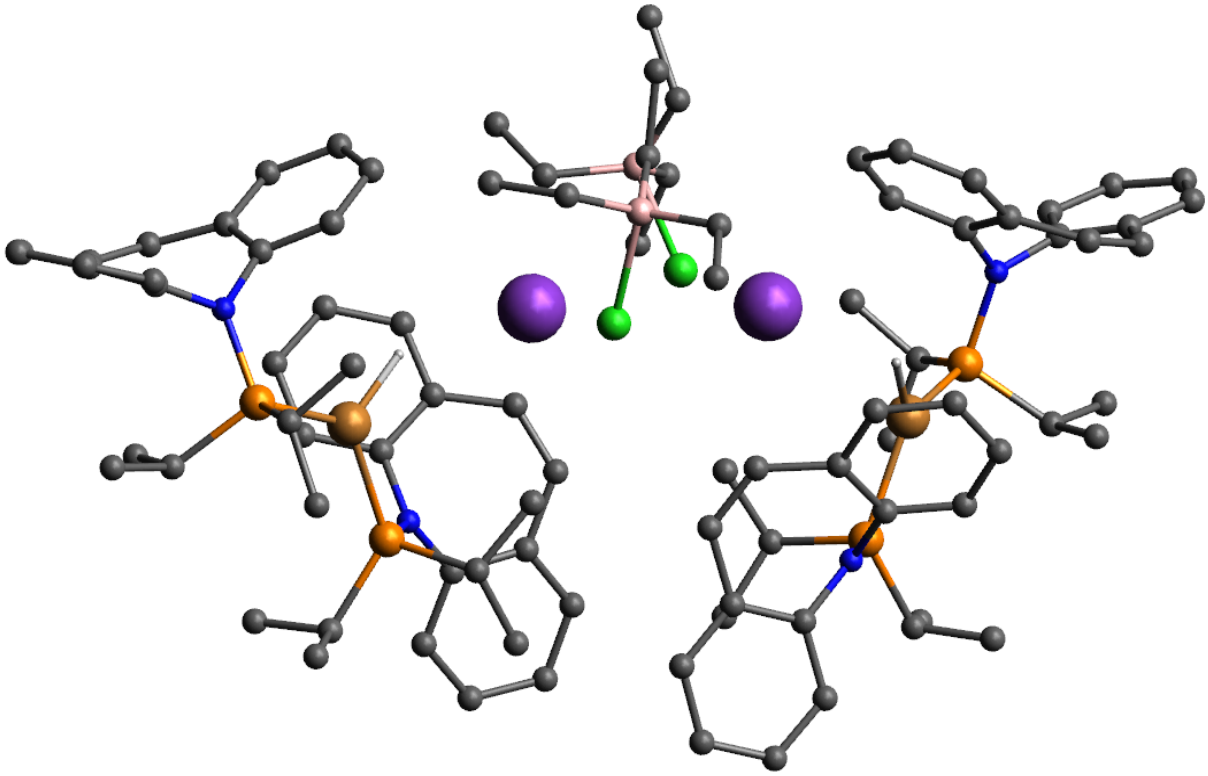

Figure S23: Optimized structure of **10d** (conformer 1) on the BP86-D4/def2-TZVP level of theory.

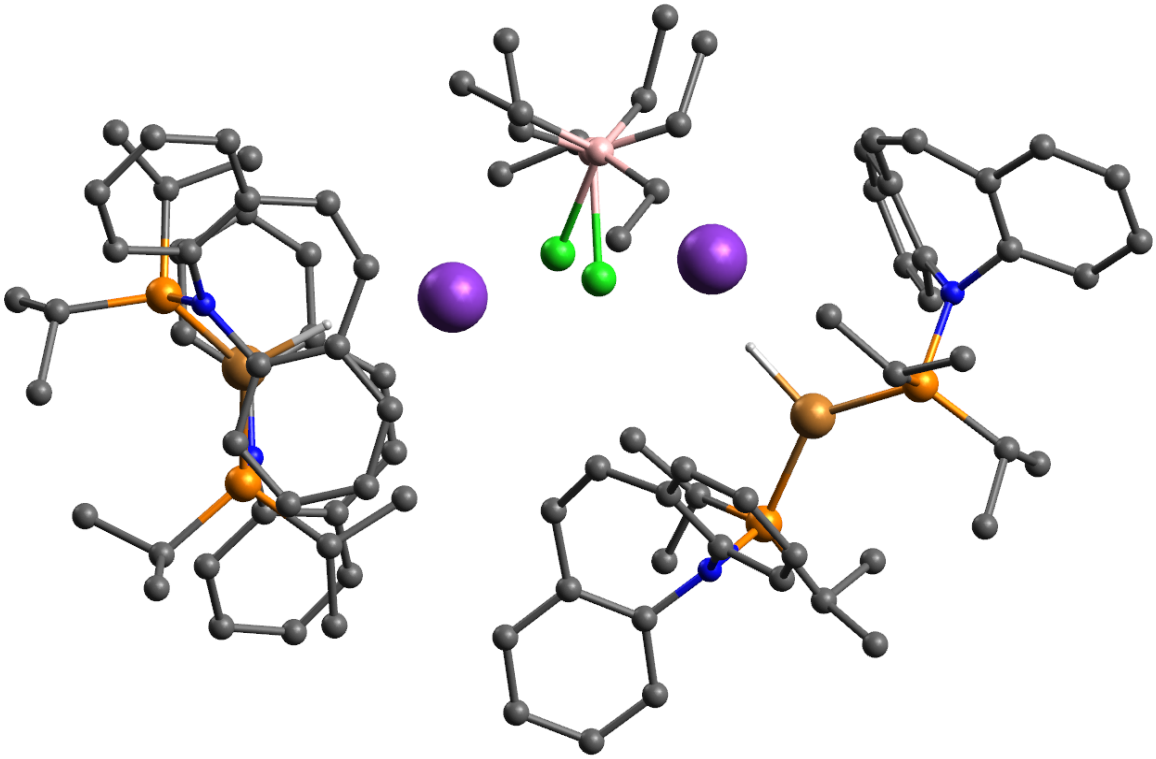

Figure S24: Optimized structure of **10d** (conformer 2) on the BP86-D4/def2-TZVP level of theory.

Figure S25 shows the calculated UV/VIS spectra of hydrido species **10a–10d**. Analysis of these low-lying transitions shows that all of them originate from excitations out of the Cu–H bond into orbitals that are mixtures of Cu-P π-bonds and π-bonds of the ligand L (see inset Figure S25). Due to the lack of the hydridic hydrogen, **10b** does not show such a low-lying absorption band and the lowest excitations correspond to ligand-centered π-π transitions. Hence, it may be concluded that **10b** is not the correct structure of the unknown intermediate **10**, *i.e.* the copper-hydrido species is not stabilized by a Cu–H…BEt_3 interaction. For dimer **10d**, the spectra of two conformers are provided: **10d**(1) is the most stable structure at 200 K we have found, **10d**(2) differs from **10d**(1) by the orientation of the ligands (see Figures S23 and S24), and is only 1.0 kcal/mol less stable than **10d**(1). The excitation energies of **10d**(2) appear, however, clearly red-shifted compared to **10d**(1) (Figure S25). This indicates that the excitation from the Cu–H bond probably has a large variability with respect to different conformations and hence, a broad band reaching beyond 400 nm is expected.

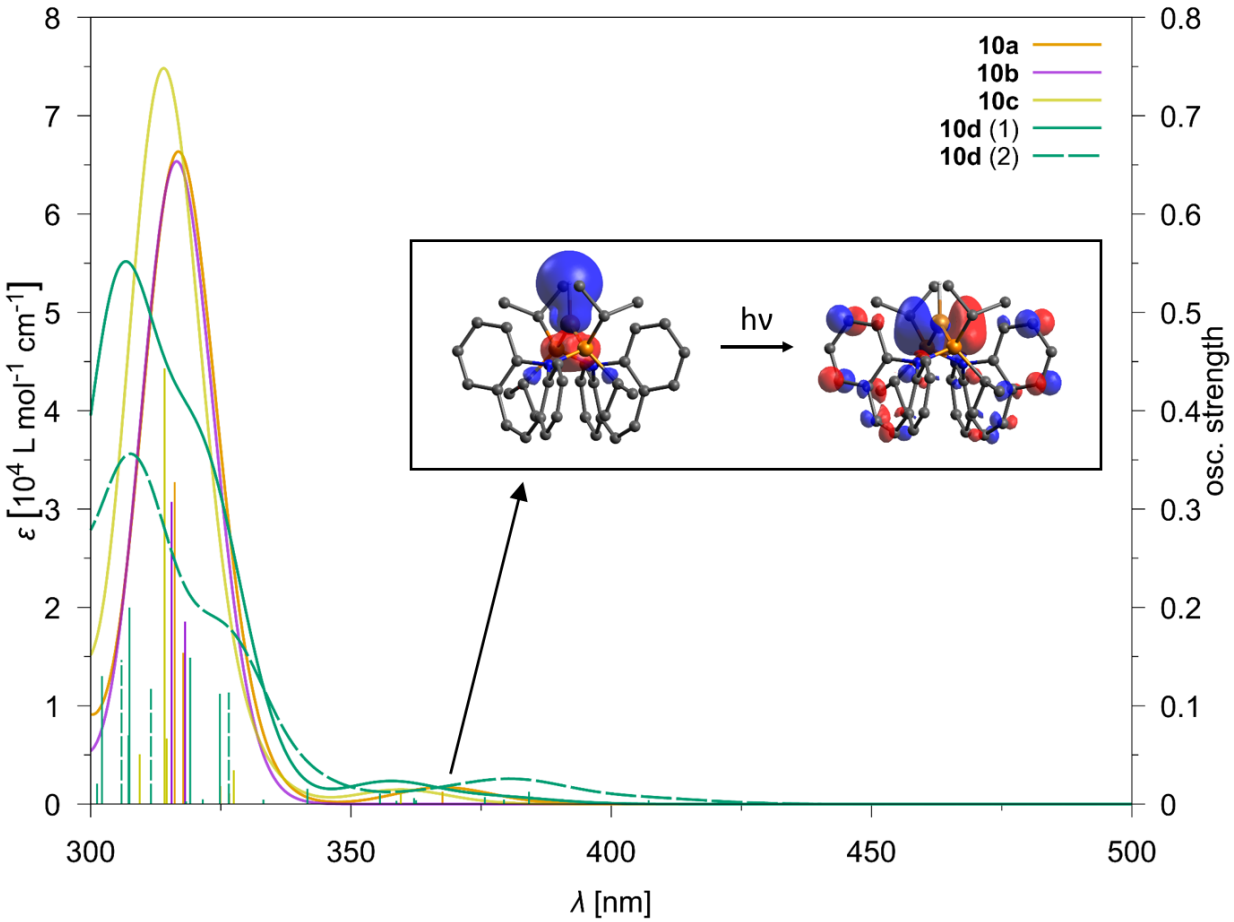

Figure S25: Simulated UV/Vis spectra (oscillator strengths and extinction coefficients) of copper hydrido species **10a–10d** on the time-dependent double-hybrid density-functional approximation level of theory. To obtain extinction coefficients, the spectra were broadened by a Gaussian of 0.2 eV full-width at half-maximum (FWHM). The calculated extinction coefficients refer to the number of monomer units. The inset shows the natural transition orbitals (NTOs) mainly (> 95 %) involved in the lowest excitation of **10a**. The low-lying (λ_{exc} > 340 nm) excited states of **10c**, **10d** (1) and **10d** (2) are connected to NTOs that closely resemble those of **10a**. Hydrogen atoms (except the copper-bound H) were removed for clarity; orbitals are plotted for an iso-value of 0.04 Bohr$^{-3/2}$.

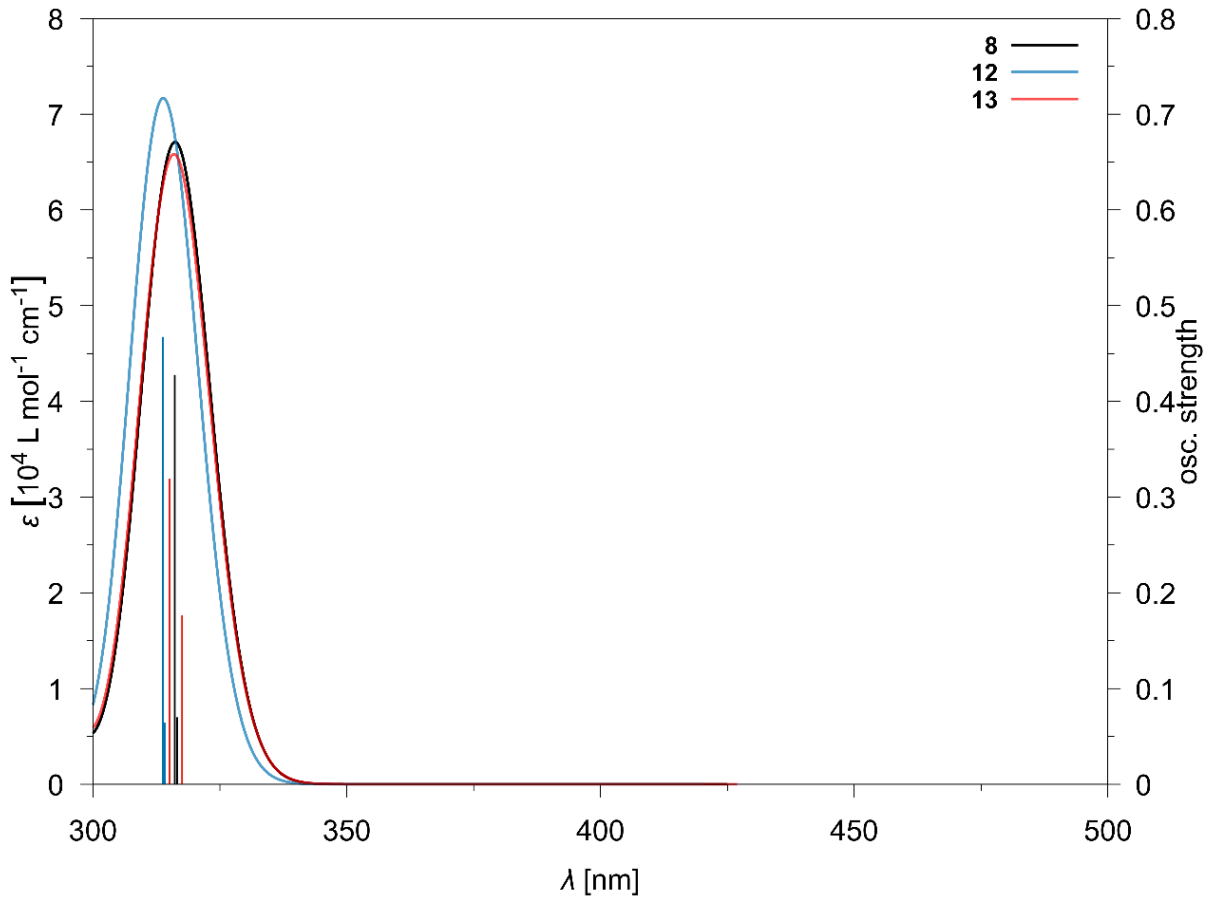

Figure S26: Simulated UV/Vis spectra (oscillator strengths and extinction coefficients) of species **8**, **12** and **13** on the time-dependent double-hybrid density-functional approximation level of theory. To obtain extinction coefficients, the spectra were broadened by a Gaussian of 0.2 eV full-width at half-maximum (FWHM).

References:

[1] A. Grasruck, G. Parla, F. W. Heineman, J. Langer, A. Herrera, S. Frieß, G. Schmid, R. Dorta Developing bulky P-alkene ligands: Stabilization of copper complexes with 14 valence electrons *New J. Chem.* **2023**, *47*, 2307.

[2] Fulmer, G. R.; Miller, A. J. M.; Sherden, N. H.; Gottlieb, H. E.; Nudelman, A.; Stoltz, B. M.; Bercaw, J. E.; Goldberg, K. I. NMR Chemical Shifts of Trace Impurities: Common Laboratory Solvents, Organics, and Gases in Deuterated Solvents Relevant to the Organometallic Chemist. *Organometallics* **2010**, *29* (9), 2176–2179.

[3] (a) Rigaku Oxford Diffraction, **2019**, CrysAlisPro Software system, version 1.171.40.53, Rigaku Corporation, Oxford, UK (compound **11**); (b) Rigaku Oxford Diffraction, **2018**, CrysAlisPro Software system, version 1.171.39.46, Rigaku Corporation, Oxford, UK (compound **13**).

[4] O. V. Dolomanov, L. J. Bourhis, R.J. Gildea, J. A. K. Howard and H. Puschmann *OLEX2:* a complete structure solution, refinement and analysis program *J. Appl. Cryst.*, **2009**, *42*, 339–341.

[5] G. M. Sheldrick *SHELXT* - Integrated space-group and crystal-structure determination *Acta Cryst. A,* **2015**, *71*, 3–8.

[6] G. M. Sheldrick Crystal structure refinement with *SHELXL Acta Cryst. C,* **2015**, *71*, 3–8.

[7] A. Thorn, B. Dittrich and G. M. Sheldrick Enhanced rigid-bond restraints *Acta Cryst. A,* **2012**, *68*, 448–451.

[8] (a) F. Neese The ORCA program system *WIREs Comput Mol Sci.* **2012**, *2*, 73–78; (b) F. Neese Software update: The ORCA program system—Version 5.0. *WIREs Comput Mol Sci.* **2022**, *12*, e1606.

[9] (a) A. D. Becke Density-functional exchange-energy approximation with correct asymptotic behavior *Phys. Rev. A* **1988**, *38*, 3098–3100; (b) J. P. Perdew Density-functional approximation for the correlation energy of the inhomogeneous electron gas *Phys. Rev. B* **1986**, *33*, 8822–8824.

[10] (a) E. Caldeweyher, C. Bannwarth, S. Grimme Extension of the D3 dispersion coefficient model *J. Chem. Phys.* **2017**, *147*, 034112; (b) E. Caldeweyher, S. Ehlert, A. Hansen, H. Neugebauer, S. Spicher, C. Bannwarth, S. Grimme A generally applicable atomic-charge dependent London dispersion correction *J. Chem. Phys.* **2019**, *150*, 154122.

[11] F. Weigend, R. Ahlrichs Balanced basis sets of split valence, triple zeta valence and quadruple zeta valence quality for H to Rn: Design and assessment of accuracy *Phys. Chem. Chem. Phys.* **2005**, *7*, 3297–3305.

[12] (a) K. Eichkorn, O. Treutler, H. Öhm, M. Häser, R. Ahlrichs Auxiliary basis sets to approximate Coulomb potentials *Chem. Phys. Lett.* **1995**, *242*, 652-660; (b) F. Weigend Accurate Coulomb-fitting basis sets for H to Rn *Phys. Chem. Chem. Phys.* **2006**, *8*, 1057–1065.

[13] (a) V. Barone, M. Cossi Quantum Calculation of Molecular Energies and Energy Gradients in Solution by a Conductor Solvent Model *J. Phys. Chem. A* **1998**, *102*, 1995–2001; (b) M. Garcia-Rates, F. Neese Effect of the solute cavity on the solvation energy and its derivatives within the framework of the Gaussian charge scheme. *J. Comput. Chem.* **2020**, *41*, 922–939.

[14] S. Grimme Supramolecular Binding Thermodynamics by Dispersion-Corrected Density Functional Theory *Chem. Eur. J.* **2012**, *18*, 9955–9964.

[15] A. Karton, A. Tarnopolsky, J.-F. Lamère, G. C. Schatz, J. M. L. Martin Highly accurate first-principles benchmark data sets for the parametrization and validation of density functional and other approximate

methods. Derivation of a robust, generally applicable, double-hybrid functional for thermochemistry and thermochemical kinetics *J. Phys. Chem. A* **2008**, *112*, 12868.

[16] (a) B. Helmich-Paris, B. de Souza, F. Neese, R. Izsák An improved chain of spheres for exchange algorithm. *J Chem Phys.* **2021**, *155*, 104109; (b) R. Izsak, F. Neese, W. Klopper Robust fitting techniques in the chain of spheres approximation to the Fock exchange: the role of the complementary space *J Chem Phys.* **2013**, *139*, 094111; (c) R. Izsak, F. Neese An overlap fitted chain of spheres exchange method *J Chem Phys*. **2011**, *135*, 144105; (d) F. Neese, F. Wennmohs, A. Hansen, U. Becker Efficient, approximate and parallel Hartree-Fock and hybrid DFT calculations. A 'chain-of-spheres' algorithm for the Hartree-Fock exchange. *Chem Phys.* **2009**, *356*, 98–109.

[17] F. Weigend, A. Köhn, C. Hättig Efficient use of the correlation consistent basis sets in resolution of the identity MP2 calculations *J. Chem. Phys.* **2002** *116*, 3175–3183.

[18] (a) I. Mayer Charge, bond order and valence in the ab initio SCF theory *Chem. Phys. Lett*. **1983**, *97*, 270–274; (b) I. Mayer Bond order and valence: Relations to Mulliken's population analysis *Int. J. Quant. Chem*. **1984**, *26*, 151–154; (c) I. Mayer Bond orders and valences in the SCF theory: a comment *Theor. Chim. Acta* **1985**, *67*, 315–322.

[19] M. Casanova-Páez, L. Goerigk Time-Dependent Long-Range-Corrected Double-Hybrid Density Functionals with Spin-Component and Spin-Opposite Scaling: A Comprehensive Analysis of Singlet-Singlet and Singlet-Triplet Excitation Energies *ChemRxiv* **2021** DOI: 10.26434/chemrxiv.14706042.v1